Controlling Maneuverability of a Bio-Inspired Swimming Robot Through Morphological Transformation

Morphology Driven Control of a Swimming Robot

Junge, Kai; Obayashi, Nana; Stella, Francesco; Della Santina, Cosimo; Hughes, Josie

DOI
10.1109/MRA.2022.3198821

Publication date
2022

Document Version
Final published version

Published in
IEEE Robotics and Automation Magazine

Controlling Maneuverability of a Bio-Inspired Swimming Robot Through Morphological Transformation

Morphology Driven Control of a Swimming Robot

By Kai Junge, Nana Obayashi, Francesco Stella, Cosimo Della Santina, and Josie Hughes

Biology provides many examples of how body adaption can be used to achieve a change in functionality. The feather star, an underwater crinoid that uses feather arms to locomote and feed, is one such system; it releases its arms to distract prey and vary its maneuverability to help escape predators. Using this crinoid as inspiration, we develop a robotic system that can alter its interaction with the environment by changing its morphology. We propose a robot that can actuate layers of flexible feathers and detach them at will. We first optimize the geometric and control parameters for a flexible feather using a hydrodynamic simulation followed by physical experiments. Second, we provide a theoretical framework for understanding how body change affects controllability. Third, we present a novel design of a soft swimming robot (Figure 1) with the ability of changing its morphology. Using this optimized

Digital Object Identifier 10.1109/MRA.2022.3198821
Date of current version: 1 September 2022

1070-9932/22©2022IEEE

feather and theoretical framework, we demonstrate, on a robotic setup, how the detachment of feathers can be used to change the motion path while maintaining the same low-level controller.

Overview

The feather star is a marine crinoid, an invertebrate with multiple soft "feathery" arms that enable swimming and maneuvering to avoid prey and feeding on drifting microorganisms [1]. These animals show many fascinating properties, including their deformable feather-like structure and cyclically actuated muscles. One of their properties, which is believed to be unique to echinoderms, is mutable collagenous tissue [2]. This enables them to drastically alter their body structure within a timescale of seconds, under direct control of the nervous system. In the case of feather stars, they use this tissue to detach their feathered arms. It is believed that this mechanism is used to distract prey and also change feather stars' dynamics to assist with evading predators [3]. This demonstrated ability to drastically alter the body morphology and passive properties to alter maneuverability is of keen interest to the robotics community. It provides inspiration for the development of robots that can utilize or change their body structure to aid their end goal or, indeed, their survival [4]. Thus, the goal of this work is to develop a feather star-inspired robot that uses an artificial equivalent of this "mutable tissue" to change its body structure. Furthermore, we present a theoretical model to investigate how the detachment of the arms affects the control and maneuverability of the design.

Within the domain of underwater bioinspired robots, there have been a number of notable examples where limbs (similar to the feathers on the feather star) and their controllers have been optimized to maximize the generated thrust [6]. This includes an octopus-inspired robot [7] and a star fish robot [8]. While these examples consider the optimization of the design of the structure to maximize thrust or behavioral range, there are limited examples of underwater robots that show considerable changes in body structure to aid control. Developing and designing robots that can utilize change in the passive properties or morphology is a key quest for embodied intelligence researchers. The role of morphology-driven control has been previously formalized [9] and shown to aid in achieving stability in legged underwater vehicles [10] and shaping the behavioral landscape of complex systems [11].

This previous work has highlighted the potential for morphology-driven control, which could be particularly beneficial in aquatic environments where fluid–structure interactions can be complex and challenging to control and exploit. To explore these capabilities, we must first create robots or structures that show significant variation in their physical structure or passive properties. To date, this has mostly been demonstrated through stiffness change in robotic systems [12] or modular reconfigurable robotic systems [13]. Using these new capabilities, we must then optimize for the morphology for optimal thrust generation [14], [15] and address how we should design the global structure before and after body changes to achieve morphology-driven control.

The feather star is a marine crinoid, an invertebrate with multiple soft "feathery" arms that enable swimming and maneuvering to avoid prey.

By developing a feather star-inspired robot with detachable feathers, we introduce a new approach to achieving significant morphological transformation in a swimming robot, which we then use to explore how body adaption can

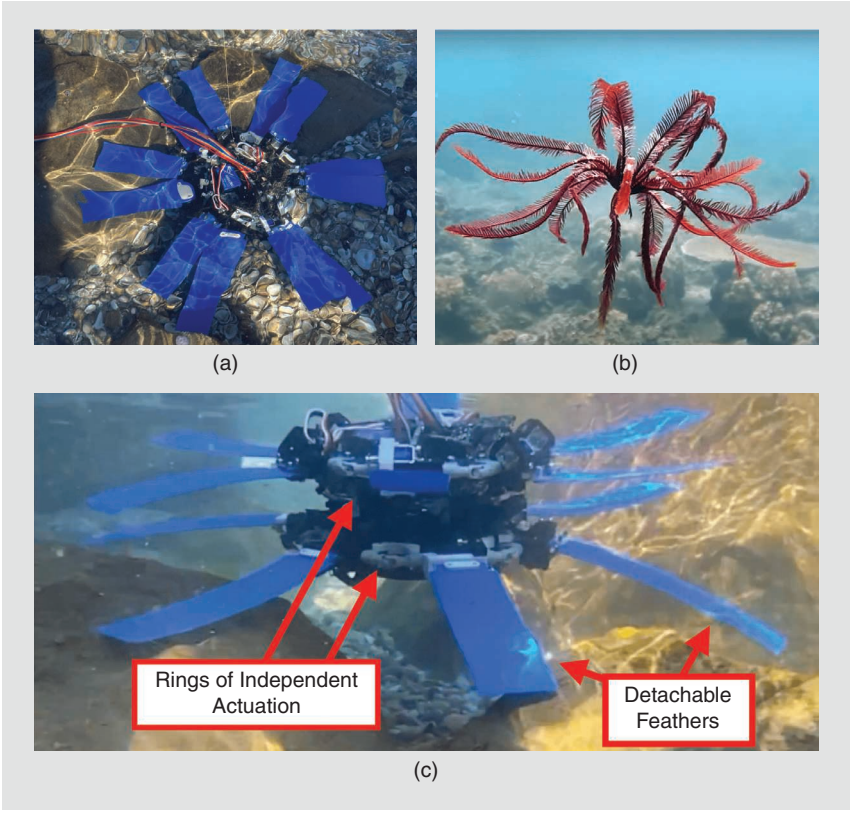

Figure 1. The (a, c) developed feather star robot with multiple actuated rings and (b)detachable feathers and its biological inspiration [5].

be used to assist with maneuvering. The novel robotic system is formed from multiple layers of actuated rings of feathers that it uses as a means of thrust generation. All the feathers in a single layer are actuated collectively, and maneuverability is achieved through adaption of the body, opposed to control of individual feathers. A mechanical system for rapid detachment has been integrated into the actuated feather rings to allow for the detachment of individual feathers.

All the feathers in a single layer are actuated collectively, and maneuverability is achieved through adaption of the body, opposed to control of individual feathers.

Due to the complex interactions between the deformable feather and water, we utilize simulation to perform a wide sweep of the control and design landscape to identify a small range of feather structures and controllers that are likely to maximize the thrust generation. By developing a custom measurement setup, we validate a small subset of these results to find the optimal feather and controller. To understand how to design the initial configuration of the robot and the choice of feathers to detach, we have developed an algorithm that utilizes the state-space representation to evaluate and determine how to change and restore the degree of controllability.

To demonstrate the contributions of this work, we experimentally validate the optimized robot structure and controllers on the robot hardware. The maneuverability of the robot is shown to alter with different configurations of the robot's feathers, following which the ability to detach the feathers on demand to alter the heading and path is shown. In the remainder of this article, we first present the methods to systematically address this problem. The novel robotic hardware is then shown, followed by the experimental results. We finish with a discussion and conclusion.

Problem Statement

Using the feather star as biological inspiration, we aim to develop a robot that utilizes feather-like structures to swim. By providing the robot with the ability to alter, or morph, its body, we want to show how changes in maneuverability can be achieved through altering the body structure. To achieve this aim, we subdivide the problem into three key goals that all seek to explore how these bioinspired components can be used to improve the capabilities of robots, as follows:

- We must explore the role of feather structures and periodic controllers in the generation of thrust through embodied interactions with the water and optimize the feathers' thrust generation through the codesign of the morphology and the controller.
- We must develop a framework for selecting the robot structure before and after the detachment of limbs to optimize the performance of the robot. In particular, we present methods for the optimization of the thrust in a particular direction and maximizing the degree of controllability of the robot.
- We must develop robotic hardware that mimics the behavior of the feather star by considering a mechanism that allows multiple feathers to be actuated simultaneously and detached at will.

The following three sections present the methods developed to address these three aspects of the problem.

Modeling and Optimization of Bioinspired Feathers

To achieve the best maneuverability, we wish to optimize the feather design parameters to maximize the thrust generated. The thrust is generated through complex interactions with the fluid and dependent on the geometry of the feather and the periodic motion at its root. To begin the optimization process, we first define the feather design parameters. Then, we use a hydrodynamics simulation model to explore the large design space, and we identify a subset of parameters that produce the largest thrust. Finally, the subset identified in simulation is further explored through real work experiments with a custom physical experimental setup.

Parametric Feather Design

The parameterized feather design and controller are shown in Figure 2(a) and (b). The geometry is defined as a rectangle, with its width w and length l as parameters. The control motion corresponds to the angular displacement at the root the feather. We evaluate only periodic motions to mimic the movements of the feather star. Consequently, the signal is fully described by the rise time t_{rise}, fall time t_{fall}, and hold time t_{hold}. We keep the amplitude constant at $A = 40^{\circ}$ to limit the size of the design search space. The 40° value is the maximum amplitude of the mechanical setup. Hence, the parameters $p_{\text{des}} = [w, l, t_{\text{rise}}, t_{\text{fall}}, t_{\text{hold}}]$ define the feather design. Polypropylene sheets of 0.4-mm thickness were chosen as the base material for the feathers, due to their flexibility and ease of fabrication using a carbon dioxide laser cutter.

Hydrodynamics Modeling

In this section, we present the model of the interaction of a single feather with the water. In particular, we first develop a discretized model for the feather, and then we define the forces exchanged between the structure and the fluid. We model a single feather as a collection of discrete flexible elements, using Simscape Multibody, where a single feather is approximated by 10 flexible beam elements [Figure 2(a)]. Each flexible element, i, consists of two masses (a and b) of

identical shape and mass, which are joined by internal springs and dampers, allowing bending [Figure 2(c)]. The first mass element, a, of the first beam element ($i = 1$) is rigidly fixed to an angular actuator at a feather's base, while the second mass element, b, of the last beam unit ($i = 10$) is a free end. All flexible elements are connected by rigid rotational joints.

The influence of the rest of the feather is imposed on each flexible element at the leading and trailing rigid joint locations as a combination of the force, F_r, and bending moment, M_r, acting on each joint, as defined in [Figure 2(c)]. The bending deformation of the feather is captured by imposing a structural bending stiffness, k_i, and damping, d_i, between the masses, a and b, which results in moments, M_{k_i} and M_{d_i}. The rotational stiffness, k_i, was calculated as EI_i/l_i, where E is the elastic modulus, I is the area moment of inertia, and l is length of the section. The elastic modulus was tuned by comparing the simulation's visual output against a physical rectangular polypropylene feather in water. The damping was approximated to be zero for all simulated joints.

Each of the masses is subject to a set of lumped external forces. Although, in the simulation, the forces are solved for each mass, for this derivation, the formulations will be expressed for the generalized flexible element, i. For each flexible element, i, the total lumped external force, F_{ext_i}, consists of gravitational force, F_{g_i}; buoyancy force, F_{b_i}; hydrodynamic force, F_{hyd_i}; and added mass force, F_{a_i}:

$$F_{ext_i} = F_{g_i} + F_{b_i} + F_{hyd_i} + F_{a_i}. \quad (1)$$

Since gravity and buoyancy always oppose each other, they can be combined as $\rho_f V_i (1 - \frac{\rho_w}{\rho_f}) u_g$, where ρ_f and ρ_w are the density of the polypropylene feather and water, respectively; V_i is the volume; g is the gravitational acceleration; and u_g is the unit vector in the direction of gravity.

The hydrodynamic force, F_{hyd}, is the total force due to the viscous interaction between the fluid and the structure. In some literature, the hydrodynamic force is decomposed into its lift and drag components, where the drag is in the direction of the relative velocity between the fluid and the body. In our simulation, we decompose the hydrodynamic force into forces in the normal and longitudinal directions of each feather element, F_{norm} and F_{long}, where these individual elements can be approximated as a rectangular prism.

By providing the robot with the ability to alter, or morph, its body, we want to show how changes in maneuverability can be achieved through altering the body structure.

The hydrodynamic opposing forces are approximated using the following equations [16]:

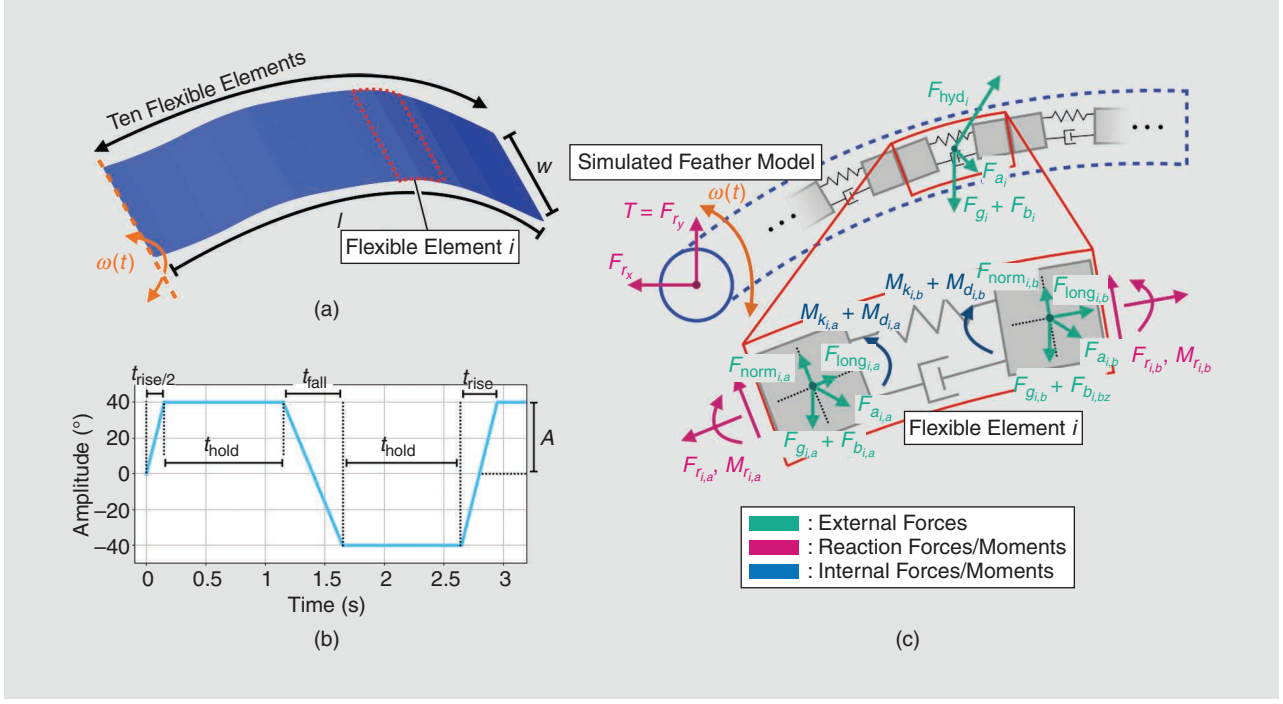

Figure 2. The (a) simulation of an actuated parameterized feather in Simscape Multibody, (b) plot of the parameterized control signal, and (c) underlying multibody model of a single feather and its interaction with water, with a close-up free-body diagram of a flexible element.

$$F_{\text{norm}_i} = \frac{1}{2} C_{\text{norm}_i} A_i \rho_w \| U_i \|^2 u_i^{\perp},$$
$$F_{\text{long}_i} = \frac{1}{2} C_{\text{long}_i} A_i \rho_w \| U_i \|^2 u_i^{\parallel}, \quad (2)$$

where the relative velocity, U_i, is decomposed into the normal and longitudinal components of the feather's longitudinal axis; A_i is the characteristic area of the feather unit; and C_{norm_i} and C_{long_i} are the hydrodynamic coefficients. These coefficients were found to be affected by the flow incidence angle. The normal component of velocity was used in this model instead of the incidence angle because for our flow regime, the streamlines of flow in the neighborhood of each feather element are bent such that the position of the separation point does not change for small angles of relative flow. The hydrodynamic coefficients for each mass of the flexible element were obtained from steady-state computational fluid dynamics simulations carried out using ANSYS software for Reynolds numbers ranging from 10 to 10^4, estimated to be fitting for such biological systems [17].

Finally, the added mass force, F_{a_i}, must also be accounted for in the total force formulation. The hydrodynamic mass force is the added mass of the movement of fluid around the accelerated body due to the action of pressure [18] and can be defined as $F_{a_i} = \rho_w A_i a_{\text{norm}_i}$, where A_i is the cross-sectional area of each element and ρ_w is the water density. The hydrodynamic added mass force is implemented on the normal component of the acceleration, a_{norm_i}, to the feather's longitudinal axis. The added mass force in the longitudinal direction was ignored for this approximation. The handling of the hydrodynamic forces captures a nonlinear feature of the fluid–structure interactions as dynamic feedback resulting from the motion of the individual elements. The actuation at the base of the feather therefore drives the kinematics and deformation dynamics.

Simulation Results

Using the hydrodynamic simulation, the design space spanned by p_{des} was explored. Specifically, we explored all combinations of geometries (w = 15–50 mm, in 5-mm increments, and l = 80–140 mm, in 20-mm increments) and all combinations of the motion parameters ($t_{\text{rise}} = 0.1, 0.5$, $t_{\text{fall}} = 0.5, 1$, and $t_{\text{hold}} = 0, 0.5, 1$ s). The geometries were chosen to match what could be used on the physical robotic setup. Each simulation was run for 10 cycles of the periodic motion, and the average thrust over one period at the base of the feather was calculated as $\bar{T} = \int_0^{t_{\text{period}}} T(t)\,dt \approx \frac{1}{n}\Sigma_n T_t$. In the remainder of the article, when referring to the "thrust," we consider this to be the average thrust $\bar{T}$ over a period.

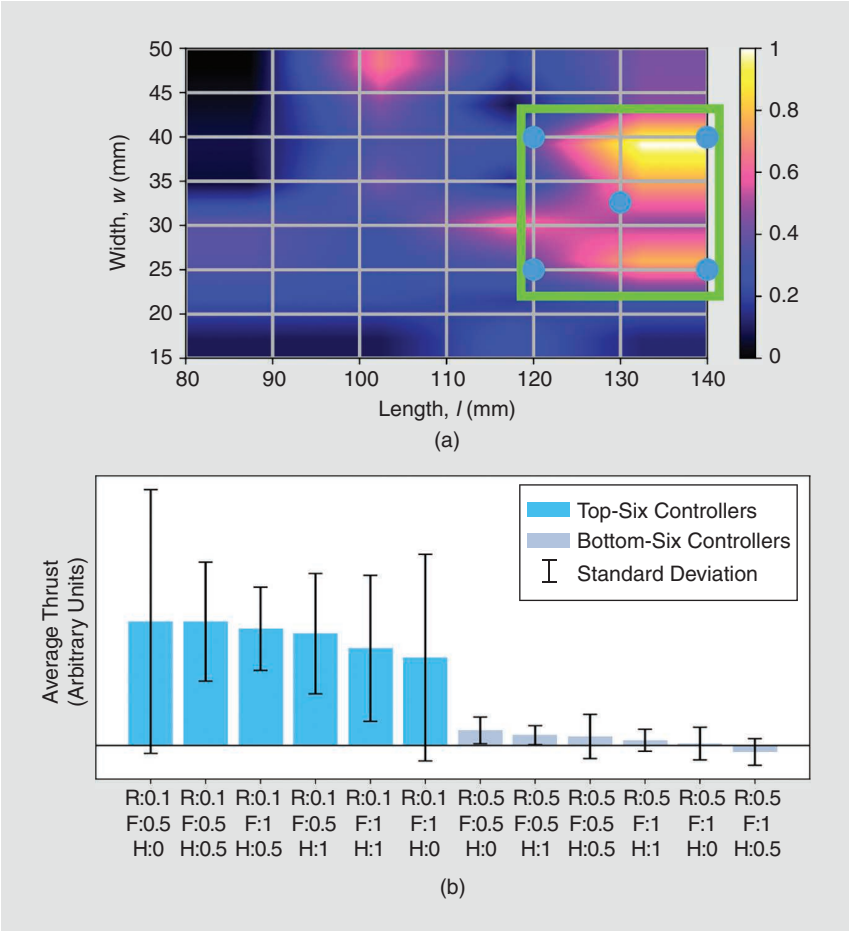

Figure 3. (a) A heat map showing the variation of the maximum $\bar{T}$ across all controllers for every feather geometry combination. A subset of l and w is identified (the green box) to be further investigated using physical experiments. (b) The simulation results for the mean and standard deviation of $\bar{T}$ across all feather geometries. The worst and best controllers are identified. R, F, and H correspond to t_{rise}, t_{fall}, and t_{hold}.

Figure 3 shows the simulation results of the thrust produced by various combinations of the parameters. These results allow us to select a smaller subspace to explore experimentally to find the optimum feather design parameter, represented as $p^{\star}_{\text{des}}$. Although the simulation allows general trends to be captured and the search space to be reduced, there remains a significant reality gap such that a small number of more costly real-world experiments must be performed. We explored five feather geometries ($[w, l] = [25,120], [25,140], [32.5,130], [40,120]$, and $[40,140]$) and seven control motions for the top six best-performing controllers and one poorly performing controller.

Experimental Exploration

To validate the simulation, we created an experimental setup (Figure 4) that

replicates the simulation. It uses a servo-powered mechanism to actuate the base of the feather, with a load cell used to measure the upward thrust. The setup ensures that there are no moments applied at the load cell so that it truly measures the upward thrust. Figure 5 shows the thrust measurements for the subset of parameters selected from the simulation results. Here, we observe the extreme sensitivity of the generated thrust for different design parameters. This highlights the complexity of optimizing the parameterized feather, even after reducing the design space to five parameters, and a need to use simulation to systematically explore and reduce the design space while not missing local maxima. From these results, some conclusions can be drawn to identify the optimal parameters p^{*}_{des}.

For the geometry, we identify the parameters $[w,l] = [40,120]$ as optimum, as they have the highest thrust recorded and the highest average thrust across different controllers. For the controller, for the optimized feather ($[w,l] = [40,120]$) we identify the parameters $[t_{\text{rise}}, t_{\text{fall}}, t_{\text{hold}}] = [0.1,0.5,0]$ as optimum. Hence, we have identified $p^{*}_{\text{des}} = [40,120,0.1,0.5,0]$. The black bar graph in Figure 5 shows the performance of the poorly performing controller in simulation. We observe that this controller is consistently poorly performing for all feather sizes, which corresponds to the simulation results. Going forward, we refer to the optimal motion parameters ($[t_{\text{rise}}, t_{\text{fall}}, t_{\text{hold}}] = [0.1,0.5,0]$) as controller 1, to the second-best motion parameters ($[t_{\text{rise}}, t_{\text{fall}}, t_{\text{hold}}] = [0.1,1,1]$) as controller 2, and to the poorly performing parameters as controller 3.

Computational Design of the Robot Structure

For the specific structure of the robot, we consider a two-layered system, where each layer has six feathers that are attached to the body radially and symmetrically (Figure 6). Therefore, in this specific design, we used $n = 6$ and $n_s = 2$. Each layer of feathers can be actuated collectively, with the angle of the base of each feather controlled in the same way as in the simulation and experimental validation. Due to the sensitivity of the thrust generation of a feather to slight changes in the controller (Figure 5), maneuverability through the control of individual feathers would be ineffective. Thus, control of the motion must be achieved with a constant controller and by utilizing changes in the body. In this section, we define how the desired change in behavior can be achieved by varying the morphology of the structure, i.e., by detaching feathers. To this end, by analyzing the controllability of the robot, we can then develop algorithms for the optimal detachment of the feathers, aimed at increasing the directional acceleration or restoring the maximal maneuverability of the design.

Since the feathers are actuated in synchrony, we can write the position $q \in \mathbb{R}^n$ of the n feathers as a function of the motor position $\sigma \in \mathbb{R}^{n_s}$. We can define the configuration of the robot with a configuration matrix $C \in \mathbb{B}^{n \times n_s}$, with $c_{i,j} = \{0,1\}$. A value of one represents the presence of a feather in the ith position for the jth motor, while a value of zero represents a detached feather. Consequently, it holds that

$$q_{\text{i,j}} = \rho c_{\text{i,j}} \sigma_{\text{j}}, \tag{3}$$

where ρ is the transmission ratio between the feather and motor coordinates. To identify designs that are able to maneuver with the minimal number of actuators, we first

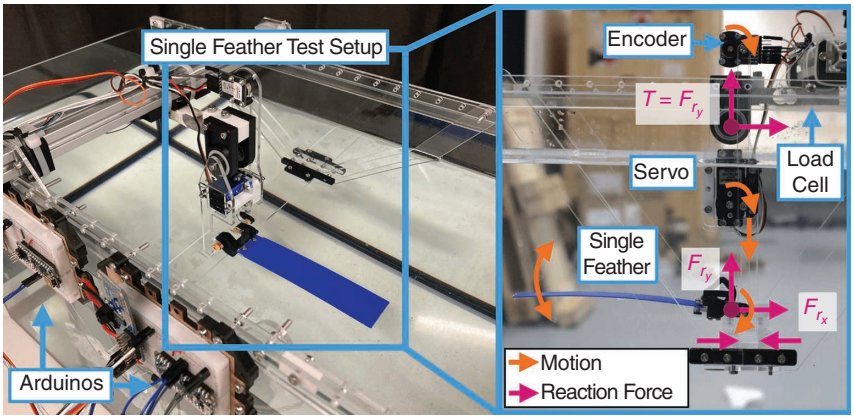

Figure 4. The experimental setup for isolating and measuring the thrust generated by feathers of different values of p_{des}.

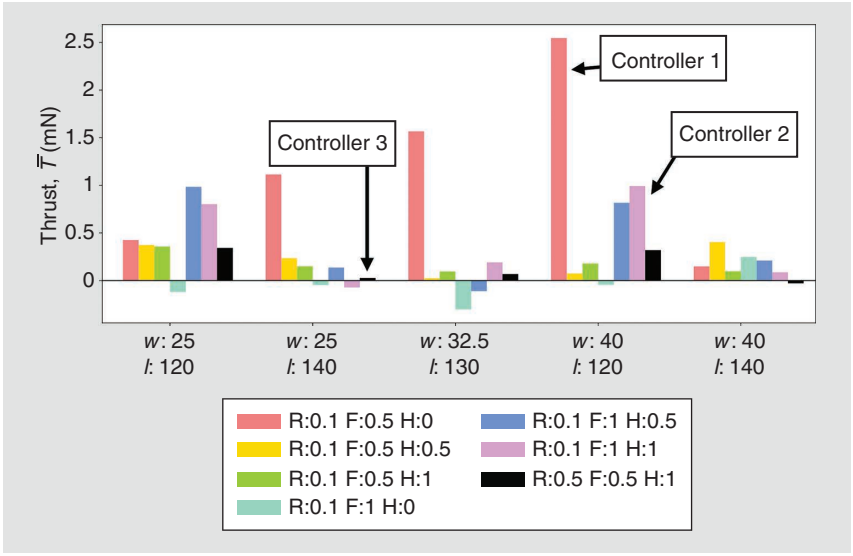

Figure 5. The experimental thrust values for a subset of feather geometries and controllers identified from simulation.

define the state-space model for a robot with a generic structure C. Then, by analyzing the role of C on the controllability of the robot, we propose the optimal configurations together with optimal policies for the detachment of the feathers.

State-Space Representation

In this section, we want to define the state-space representation of a robot defined by the configuration matrix C, aiming at controlling a nonholonomic underactuated system in a 3D space and with $n_s < n$ motors. The equations of motion can be written in the inertial frame, indexed with W, or in the body frame, referenced with B, as in Figure 6. The position of the B frame in W coordinates is defined by the translation vector r with components $[x, y, z]$ and by the Euler angles $[\phi, \theta, \psi]$ defining the roll, pitch, and yaw angles, respectively. Using these coordinates, we can write the transformation matrix between the reference systems W and B. Finally, the angular velocity of the robot is described as $\omega_{BW} = [p, s, v]$, denoting the angular velocity of frame B in the frame W, with components p, s, and v in the body frame. Therefore, the Newton–Euler equations for the whole robot are

$$
\begin{aligned}
m\ddot{r}_W &= \begin{pmatrix} 0 \\ 0 \\ -(m - m_w)g \end{pmatrix}_W + \begin{pmatrix} 0 \\ 0 \\ T_{tot} \end{pmatrix}_B, \\
I\begin{pmatrix} \dot{p} \\ \dot{s} \\ \dot{v} \end{pmatrix}_B &= \begin{pmatrix} \tau_{pitch} \\ \tau_{roll} \\ 0 \end{pmatrix}_B - \begin{pmatrix} p \\ s \\ v \end{pmatrix}_B \times I\begin{pmatrix} p \\ s \\ v \end{pmatrix}_B,
\end{aligned}
\tag{4}
$$

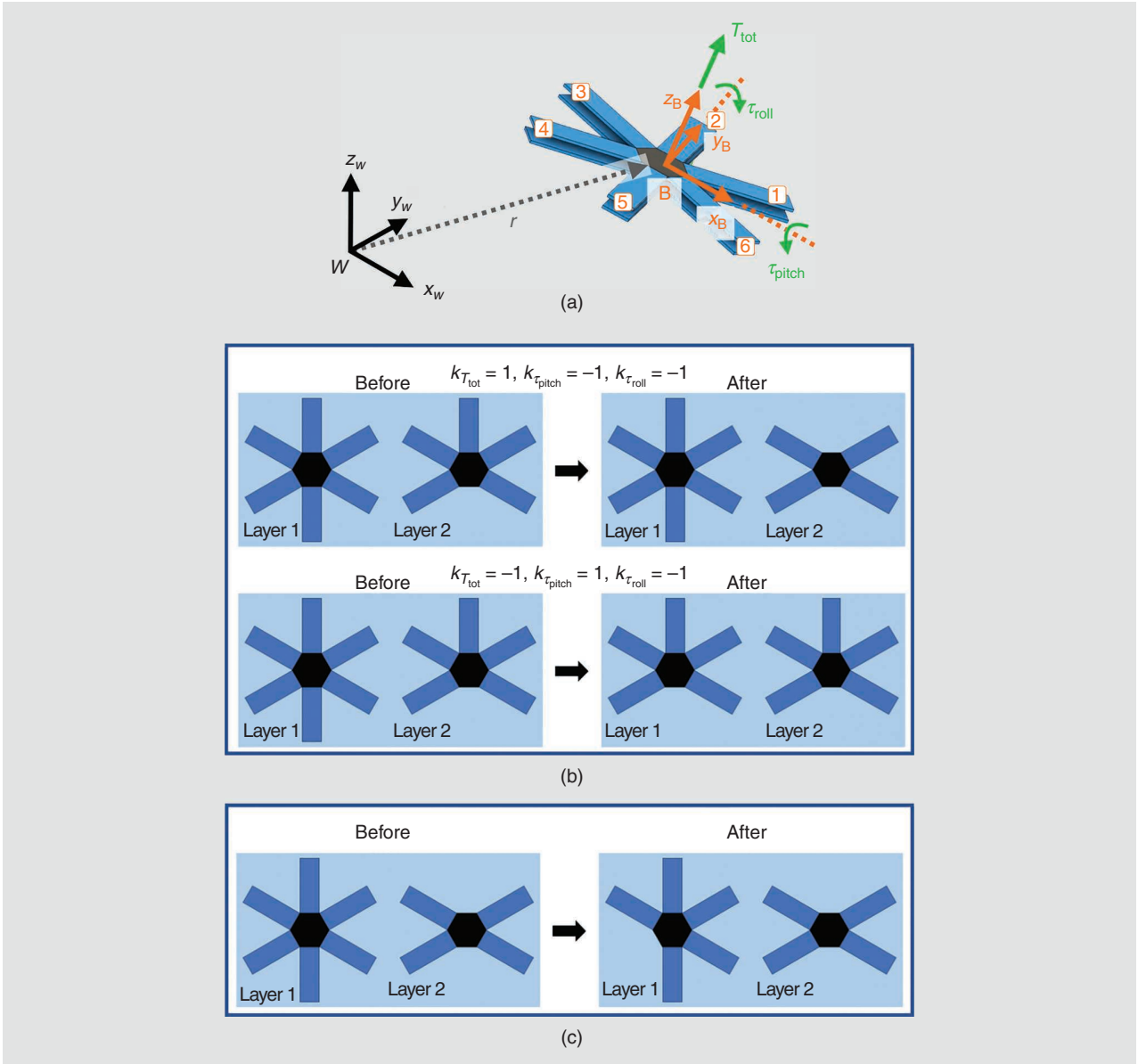

Figure 6. (a) The schematic representation of the abstracted robot. The control algorithm allows for altering the level of controllability by (b) increasing the directional thrust and (c) restoring maneuverability.

where I represents the inertia of the body and m, and m_w are the mass of the robot and the displaced water respectively.

Each feather is actuated following a periodic oscillatory trajectory, producing an average thrust $\bar{T}$ directed upward in the plane of motion, as described in the "Modeling and Optimization of Bioinspired Feathers" section. Since all feathers on the same layer are moved in synchrony, the thrust produced by a generic feather on the jth layer can be described as $\bar{T}_j$. Consequently, the forces produced by the whole robot on the environment can be written as

$$\begin{aligned} T_{\text{tot}} &= \sum_i^n \sum_j^n c_{\text{i,j}} \bar{T}_{\text{j}}, \\ \tau_{\text{pitch}} &= d \sum_j^n \bar{T}_{\text{j}} (c_{2\text{j}} - c_{5\text{j}} + \frac{1}{2}(-c_{1\text{j}} - c_{3\text{j}} + c_{4\text{j}} + c_{6\text{j}}), \\ \tau_{\text{roll}} &= d \frac{\sqrt{3}}{2} \sum_j^n \bar{T}_{\text{j}} (-c_{1\text{j}} + c_{3\text{j}} + c_{4\text{j}} - c_{6\text{j}}), \end{aligned} \tag{5}$$

where d represents the distance between the center of mass and the location of the resulting force for each feather. In the following, the vector of inputs $u_1 = [T_{\text{tot}}, \tau_{\text{pitch}}, \tau_{\text{roll}}]^\top$ will be used to simplify the physical intuition. However, the vector u_1 can be mapped back to the motor activation input $u_2 = [\bar{T}_1, ..., \bar{T}_{\text{n}_\text{s}}]^\top$ through the mapping $M = (\partial u_1 / \partial u_2)$ such that it holds that $u_1 = M u_2$. Thanks to this mapping, we can write the resulting forces on the robot, given the configuration C and the activation state of the motors.

We can then rewrite the system in state-space form. The state of the system is given by the position and velocity of the center of mass and the orientation and the angular velocity, $x = [x, y, z, \phi, \theta, \psi, u, v, w, p, s, v]^\top = [x_1, x_2, x_3, x_4, x_5, x_6, x_7, x_8, x_9, x_{10}, x_{11}, x_{12}]^\top$, while the control input is $u = [\bar{T}_1, ..., \bar{T}_{\text{n}_\text{s}}]$. Therefore, the complete nonlinear system becomes

$$\dot{x} = \begin{pmatrix} x_7 \\ x_8 \\ x_9 \\ x_{10} \\ x_{11} \\ x_{12} \\ x_{12} x_8 - x_{11} x_{10} - g \sin(x_5) \\ x_{10} x_9 - x_{12} x_7 + g \sin(x_4) \cos(x_5) \\ x_{11} x_7 - x_{10} x_8 + g \cos(x_4) \cos(x_5) - \dfrac{T_{\text{tot}}}{m} \\ \dfrac{I_{\text{y}} - I_{\text{z}}}{I_{\text{x}}} x_{12} x_{11} + \dfrac{\tau_{\text{roll}}}{I_{\text{x}}} \\ \dfrac{I_{\text{z}} - I_{\text{x}}}{I_{\text{y}}} x_{10} x_{12} + \dfrac{\tau_{\text{pitch}}}{I_{\text{y}}} \\ \dfrac{I_{\text{x}} - I_{\text{y}}}{I_{\text{z}}} x_{10} x_{11} \end{pmatrix}. \tag{6}$$

Using the nonlinear state-space representation, we define a linearization around the hovering configuration, and we study the controllability of the structure as a function of C. In the linearized state around the hovering condition, $\theta = 0$, $\phi = 0$, and $\sum T = (m - m_w) g$ holds. Therefore, the equations of motion can be written as

$$\dot{x} = Ax + Bu_1 = Ax + BMu_2. \tag{7}$$

Given A and B, we can study the degrees of controllability of the configuration by evaluating the rank of the controllability Gramian $\text{rank}(\text{gram}(A, BM))$ of the system [19]. A robot with a degree of controllability of n is able to exert forces along n independent directions. This metric is then ultimately linked to the robot's behavior, as it informs us of how many independent directions the robot can accelerate or react to disturbances in. Maximizing such a metric leads to a robot that can react to any disturbance and that is fully controllable [20].

Optimal Detachment

In this section, we present how the detachment of feathers can be optimized to increase the performance of the robot in one specific task, such as escaping a predator. In this scenario, we want our robot to move as quickly as possible in one direction. Considering that, the robot configuration can be optimized to produce the maximum directional thrust by solving the discrete optimization problem

$$\begin{aligned} &\underset{c_{\text{i,j}} \in \{0,1\}}{\text{argmax}} \; k_{T_{\text{tot}}} \mid T_{\text{tot}} \mid + k_{\tau_{\text{roll}}} \mid \tau_{\text{roll}} \mid + k_{\tau_{\text{pitch}}} \mid \tau_{\text{pitch}} \mid, \\ &\text{s.t.} \quad T_{\text{j}} \in \{-\overline{T_{\text{j}}}, 0, \overline{T_{\text{j}}}\}, \end{aligned} \tag{8}$$

where $[k_{T_{\text{tot}}}, k_{\tau_{\text{roll}}}, k_{\tau_{\text{pitch}}}] \in \mathbb{R}^3$ are weight parameters that describe the desired behavior and $T_{\text{tot}}, \tau_{\text{roll}}$, and τ_{pitch} are defined as in (5). Note that the optimization is solved by evaluating a combinatorial problem on the subset of binary variables $c_{\text{i,j}}$ that have value one in the current configuration.

On the other hand, a feather can be detached to restore a higher degree of controllability. In this case, the optimal feather to detach is found by solving the optimization problem

$$\begin{aligned} &\underset{c_{\text{i,j}} \in \{0,1\}}{\text{argmax}} \quad \text{rank}(\text{gram}(A, B)), \\ &\qquad\qquad \text{s.t} \quad T_{\text{j}} = \overline{T_j}. \end{aligned} \tag{9}$$

Through the evaluation of the controllability Gramian matrix, we can distinguish among designs with the same $\text{rank}(M_C)$, where M_C represents the controllability matrix. In Figure 6(b) and (c), we show how, through the mathematical model of the design, we can optimize the configuration of the robot for a desired behavior. The results from the presented algorithm are used as a framework for the experiments presented in "Experimental Results" section.

Robotic Hardware Design

The robot is a multilayered system. Each layer has six feathers arranged regularly in a hexagonal pattern [shown in Figure 7(a)]. A servo motor is located in the center of the layer and actuates two feather holders on opposite sides through a linkage mechanism. On either side of the holder

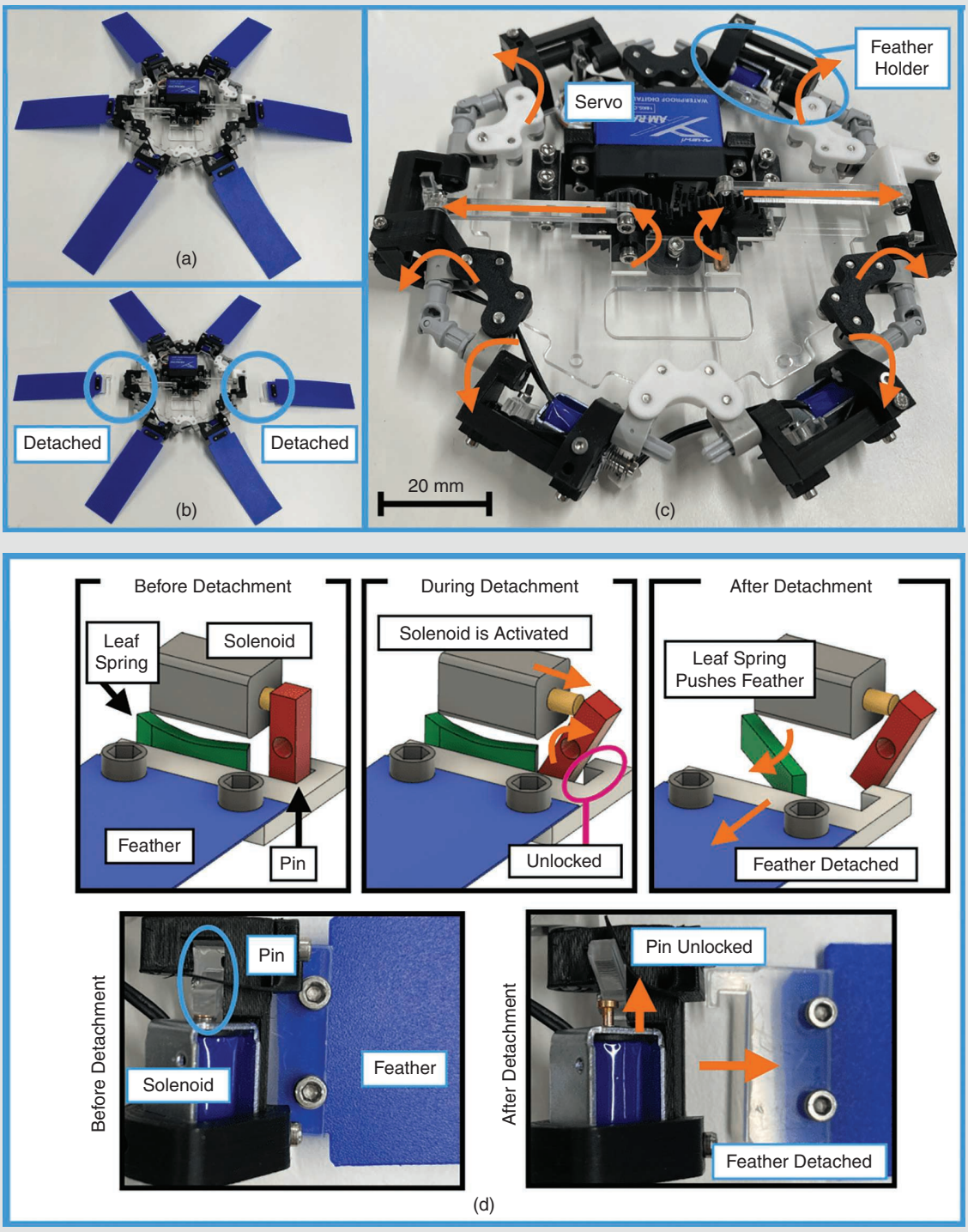

Figure 7. The mechanical design of the robot, focusing on the single layer. (a) A single layer with all feathers attached. (b) A single layer with two feathers detached. (c) The actuation mechanism for moving six feather holders with one servo motor. (d) The detachment mechanism using a solenoid.

directly actuated by the servo motor, an additional holder is located, which is connected by a universal joint. This mechanical configuration results in all holders being actuated in synchrony [see Figure 7(c)].

A feather shape is fabricated by cutting a polypropylene sheet on a laser cutter. Each feather is bolted to an acrylic connector, which can be slotted into the feather holder. Each holder can be equipped with a solenoid that drives the detachment mechanism [Figure 7(b) shows how feathers can be attached to or detached from the layer]. The feather detachment mechanism is described in Figure 7(d). When a solenoid attached on the feather holder is energized, a pin holding the feather in place is unlocked, allowing a leaf spring (a 3D-printed flexure) to push out the feather from the holder. This allows feathers to be detached rapidly and on demand.

In this experiment, two layers were fabricated and assembled (see Figure 1). Electrical wires form the servo motor, and solenoids connect the waterproofed robot to the Arduino microcontroller located outside of the water. Solenoids are energized through MOSFETs, which can be turned on and off via the Arduino. The Arduino is connected to a PC, where the feather detachment and the servo motion profile are commanded by a human operator.

Experimental Results

Feather Optimization

To demonstrate and experimentally validate the optimization of a single feather on the robot, a single ring of the robot was tested with different feathers and controllers. The single ring was tested with the "optimized" feathers (120 × 40 mm) and feathers with the same area but longer (192 × 25 mm) to provide a baseline. For these two robot configurations, three different controllers were tested: the two top controllers from the experimental validation of the optimized feather (Figure 5), i.e., controllers 1 and 2, and controller 3, which was poorly performing in both simulation and the single feather experiment. The neutrally buoyant robot was placed in a downward-facing configuration, with a thin rod placed through the center of its body to constrain its motion to allow for comparison among experiments. For each combination of feather geometry and controller, the robot was recorded swimming downward until the bottom of the tank was reached (or the time exceed 1 min) for five repetitions, where the average swimming velocity was obtained (Figure 8).

The results, in Figure 5, show that the optimized feathers significantly outperform the baseline feathers, with the speeds generated by the top two controllers offering more than a 60% increase relative to the baseline feathers. The experiments reinforce that controller 1 shows the greatest thrust generation and, hence, velocity. However, the relative performance of controller 2 is poorer than expected, with controller 2 showing a velocity, on average, 10% lower than controller 1. Compared to the single-feather case, the servo motor on the robot must exert a higher torque to move all the feathers. Without a sufficiently long hold time, the true position of the servo motor in some cases does not reach the desired position (for both up and down strokes). Hence, we believe that controller 2, with a longer hold time, is less susceptible to environmental disturbances and noise, which cause the up and down strokes to not meet the desired angles. In addition, it was clearly observed that when using controller 1, the true feather amplitude is less than the servo motor demand position ($A = 40^{o}$). This is because of the lack of hold time in controller 1, which means the servo demand position direction is reversed before the motor has time to reach it. In comparison to the top-performing controllers, controller 3 struggled to produce any downward thrust for both feather geometries.

Single-Ring Control of Motion

To demonstrate and explore the degree of controllability, we first present one single layer of the robot. While the range of motion is lower than for multiple layers, it allows the concepts to be explored on lower complexity hardware. To demonstrate how varying the body structure leads to different behaviors, we first show the motion of the robot with different fixed feather configurations [Figure 9(a)–(d)]. For these and all following experiments we aimed to perform them in the center of the tank as much as possible, and if the sides of the tank influenced the experiment, the experiment was repeated. These results show that different robot configurations lead to different motions and directions of swimming. Fully symmetric designs [Figure 9(c)] and partially symmetric designs that produce a net thrust at the center of the layer [Figure 9(d)] lead to the robot swimming in a straight line, whereas asymmetric designs [Figure 9(a) and (b)] allow for gradual turning arcs.

To demonstrate how we can use this variation in motion with body shape, we extend the experiments to include the detachment of feathers to transition among different motions. As shown in Figure 9(e)–(h), the detachment of feathers results in a change in heading of the robot. By altering both the starting configuration and the selection of feathers to be detached, the motion before and after detachment can be controlled. Figure 9(e)–(h) shows how the robot transitions from one stable motion to another stable motion, where the change is caused by feather detachment. These experiments demonstrate that even with the same controller, the change in body (detachment) leads to a change in motion. In some cases, the robot moves close to the edge of the tank, where the fluid behavior may be more complex. Although the dominant effect on the maneuverability is still from the feather detachment, in open water, the exact trajectory may differ.

Two-Layer Robot Demonstration

The full two-layer robot allows for a complete demonstration of the analytical results described by the optimization problems in

(8) and (9). These optimization problems reflect the need to select the optimal detachment of feathers to increase the thrust in one direction or to maximize the controllability of the structure, respectively. In particular, we provide an example of starting in a horizontal configuration and moving in the vertical direction. For this case, we consider solving the two different optimization problems and assess how the solutions lead to changes in controllability or speed. In option 1, we apply the optimization problem described in (9). We are therefore maximizing the possibility to control the structure, with the resulting structure able to move linearly, as shown in Figure 10(a), and to turn, as shown in Figure 10(b). However, this possibility in control comes at the cost of lower acceleration in both motions.

On the other hand, in option 2, we apply (8), with the parameters of the cost function being $[k_{T_{\text{tot}}}, k_{\tau_{\text{roll}}}, k_{\tau_{\text{pitch}}}] = [1, -1, -1]$. We are therefore maximizing the total thrust produced by the structure while penalizing any turning motion. For this optimization problem, the solution is to detach the asymmetric feather so that, when actuated, both layers will produce thrust in the same direction. These results are reflected in Figure 10(c). These results show that with option 2, a speed increase of over 60% can be achieved with the optimal feather detachment. Thanks to (8) and (9), we are therefore able to intuitively specify the desired behavior of the robot by tuning few parameters in the cost function of the optimization problem, and the optimal feather detachment will be computed, considering the internal dynamics of the system described in (7).

Discussion and Conclusion

Biology provides many examples of mechanisms by which adaptation of the body can be used to simplify complex functions or enable otherwise impossible functionality. The feather star provides a number of fascinating examples. Using this as an inspiration, we have developed a robot with feathers that utilizes these passive structures for swimming and the detachment of the feathers to change its structure. Utilizing modeling and experimental results, we have optimized the morphology and control of these feathers and developed a theoretical framework

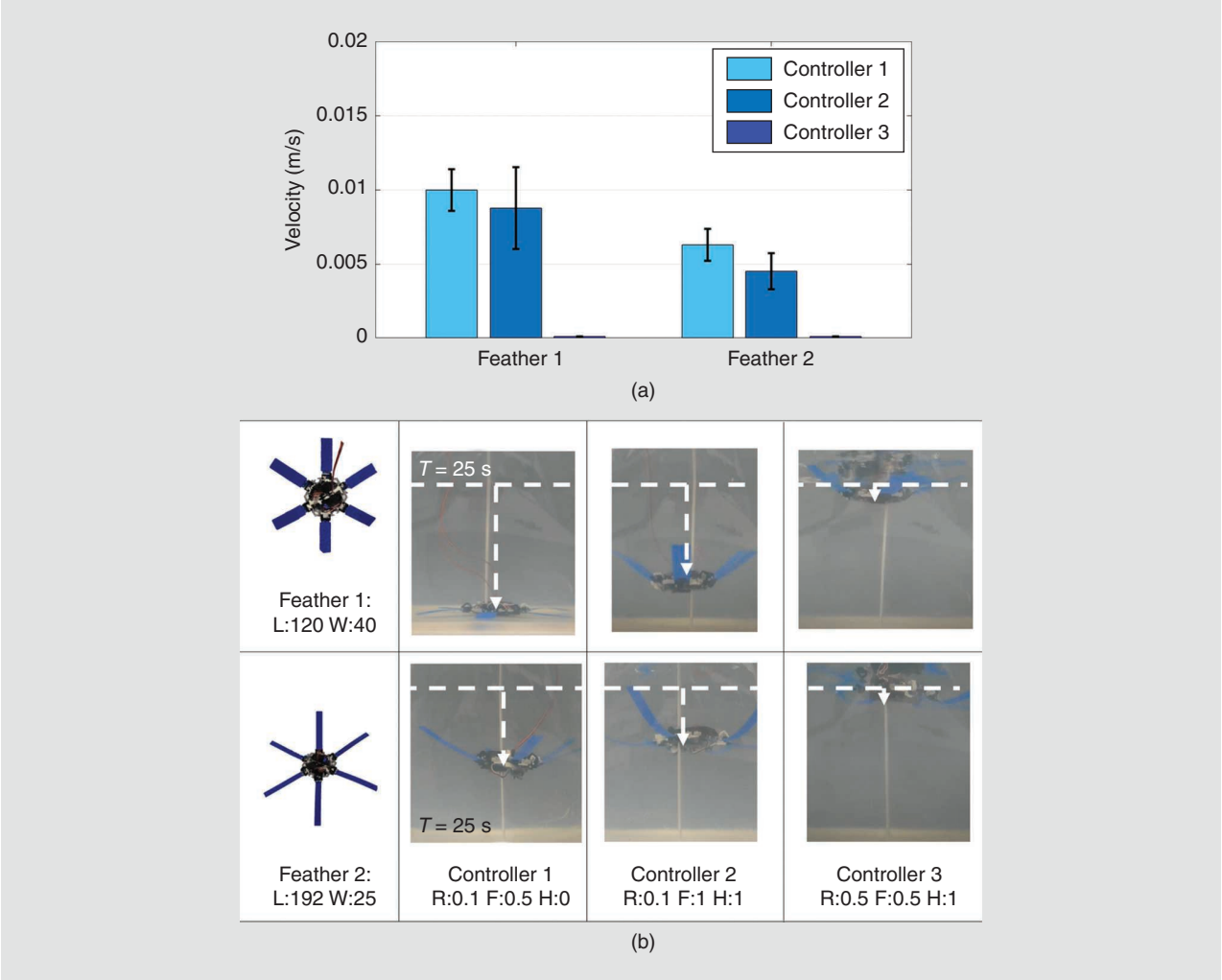

Figure 8. A comparison of the optimal feathers (120 × 40) and baseline with the same area (192 × 25) for three different controllers. Each experiment was repeated five times, with the velocity and standard deviation presented.

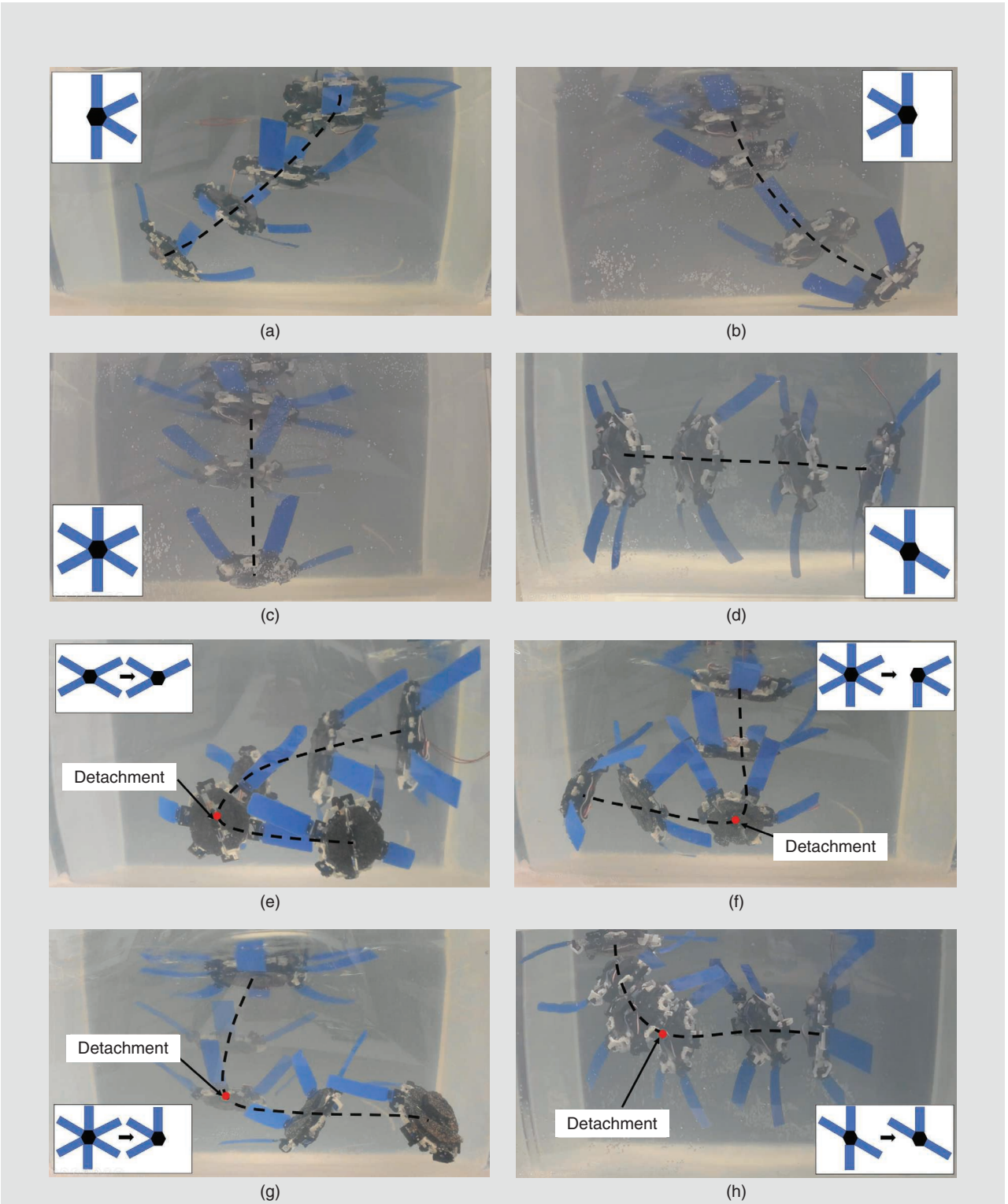

Figure 9. The maneuverability of the robot (a–d) for different feather configurations and example motions of the robot (e–h) showcasing the change of heading when feathers are detached. In particular, the detachment of the feathers is computed by solving (8), with the cost function parameters $[k_{\tau_{\text{tot}}}, k_{\tau_{\text{roll}}}, k_{\tau_{\text{pitch}}}] = [0, 0, 1], [0, 0.1, -1], [0, -0.1, 1]$, and $[0, 1, 0]$ for (e)–(h), respectively.

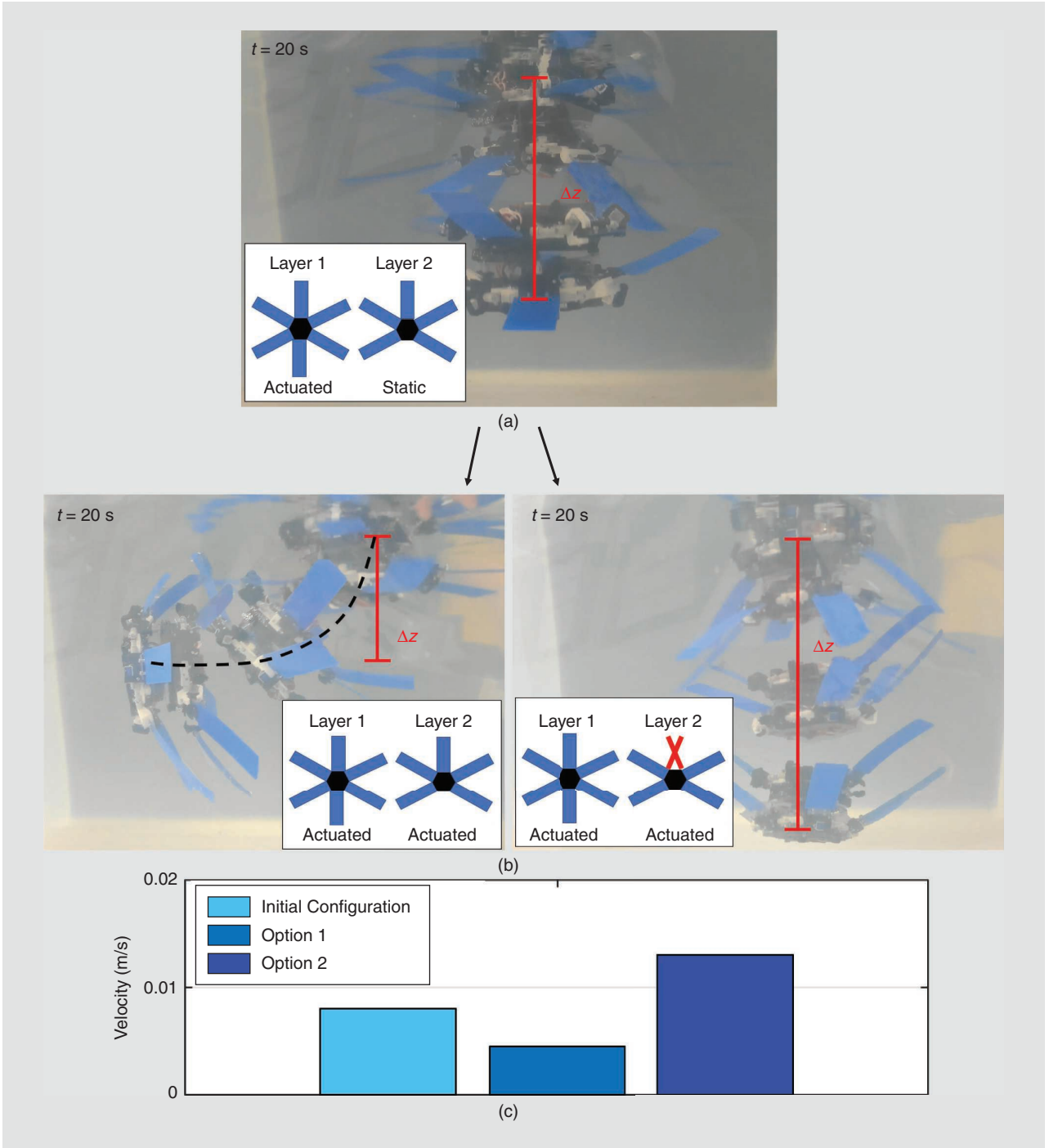

Figure 10. The increased performance arising from the optimal detachment of a feather. Starting from (a) the initial configuration, we can achieve (b) a higher speed in the z direction by detaching one feather and actuating both layers. (c) A comparison of the performance results.

for when and how to alter the body to achieve a change in functionality.

The results presented show an initial exploration of using "detachment" inspired by mutable tissues as a means of changing the body. This allows the robot to have a time-varying design space. Expanding this capability to allow not only detachment but also retrieval or growth would further expand this concept and bridge the gap to reality. In addition, increasing the physical complexity of the robot, for example, increasing the number of layers, would allow a larger and more complex control space to be explored. Testing and evaluating the robot in a large body of water would also enable longer trajectories to be studied and provide a means of evaluating the maneuverability of the system

with fewer edge effects from the tanks walls. Considering the feathers, even using the crude approximation of rectangular structures, we have demonstrated that there is a complex relationship between among morphology, control, and resultant thrust. Further exploring this study to consider other geometries, materials, and complex structures (for example, bristles on the arms) would also extend this exploration.

Acknowledgment

This project was partially funded by the European Union's Horizon 2020 research and innovation program, under Marie Skłodowska Curie grant 945363. Kai Junge, Nana Obayashi, and Francesco Stella contributed equally to this work.

References

[1] C. G. Messing, "Brooding and paedomorphosis in the deep-water feather star Comatilia iridometriformis (Echinodermata: Crinoidea)," *Mar. Biol.*, vol. 80, no. 1, pp. 83–91, 1984, doi: 10.1007/BF00393131.

[2] I. C. Wilkie, M. Sugni, H. S. Gupta, M. D. Candia Carnevali, and M. R. Elphick, "The mutable collagenous tissue of echinoderms: From biology to biomedical applications," in *Soft Matter Systems for Biomedical Applications*, L. Bulavin and N. Lebovka, Eds., New York, NY, USA: Springer-Verlag, 2021, ch. 1, pp. 1–33, doi: 10.1039/9781839161124-00001.

[3] A. Stevenson, F. J. Gahn, T. K. Baumiller, and G. D. Sevastopulo, "Predation on feather stars by regular echinoids as evidenced by laboratory and field observations and its paleobiological implications," *Paleobiology*, vol. 43, no. 2, pp. 274–285, 2017, doi: 10.1017/pab.2016.39.

[4] C. Laschi and M. Cianchetti, "Soft robotics: New perspectives for robot bodyware and control," *Frontiers Bioeng. Biotechnol.*, vol. 2, p. 3, Jan. 2014, doi: 10.3389/fbioe.2014.00003.

[5] Nat Geo Wild, *Feather Stars and Their Animal Invaders*. (Aug. 2018). [Online Video]. Available: https://www.youtube.com/watch?v=OyketlthVWg&t=2s

[6] M. Calisti, G. Picardi, and C. Laschi, "Fundamentals of soft robot locomotion," *J. Roy. Soc. Interface*, vol. 14, no. 130, p. 20,170,101, 2017, doi: 10.1098/rsif.2017.0101.

[7] M. Cianchetti, M. Follador, B. Mazzolai, P. Dario, and C. Laschi, "Design and development of a soft robotic octopus arm exploiting embodied intelligence," in *Proc. 2012 IEEE Int. Conf. Robot. Autom.*, pp. 5271–5276, doi: 10.1109/ICRA.2012.6224696.

[8] T. Du, J. Hughes, S. Wah, W. Matusik, and D. Rus, "Underwater soft robot modeling and control with differentiable simulation," *IEEE Robot. Autom. Lett.*, vol. 6, no. 3, pp. 4994–5001, Jul. 2021, doi: 10.1109/LRA.2021.3070305.

[9] R. M. Füchslin et al., "Morphological computation and morphological control: Steps toward a formal theory and applications," *Artif. life*, vol. 19, no. 1, pp. 9–34, 2013, doi: 10.1162/ARTL_a_00079.

[10] G. Picardi, H. Hauser, C. Laschi, and M. Calisti, "Morphologically induced stability on an underwater legged robot with a deformable body," *Int. J. Robot. Res.*, vol. 40, no. 1, pp. 435–448, 2021, doi: 10.1177/0278364919840426.

[11] M. Garrad, J. Rossiter, and H. Hauser, "Shaping behavior with adaptive morphology," *IEEE Robot. Autom. Lett.*, vol. 3, no. 3, pp. 2056–2062, Jul. 2018, doi: 10.1109/LRA.2018.2807591.

[12] Y.-J. Park, T. M. Huh, D. Park, and K.-J. Cho, "Design of a variable-stiffness flapping mechanism for maximizing the thrust of a bio-inspired underwater robot," *Bioinspiration Biomimetics*, vol. 9, no. 3, p. 036002, 2014, doi: 10.1088/1748-3182/9/3/036002.

[13] S. Li et al., "Scaling up soft robotics: a meter-scale, modular, and reconfigurable soft robotic system," *Soft Robot.*, vol. 9, no. 2, pp. 324–336, 2022, doi: 10.1089/soro.2020.0123.

[14] N. Obayashi, C. Bosio, and J. Hughes, "Soft passive swimmer optimization: From simulation to reality using data-driven transformation," in *Proc. 2022 IEEE 5th Int. Conf. Soft Robot. (RoboSoft)*, pp. 328–333, doi: 10.1109/RoboSoft54090.2022.9762148.

[15] F. Stella, N. Obayashi, C. D. Santina, and J. Hughes, "An experimental validation of the polynomial curvature model: identification and optimal control of a soft underwater tentacle," *IEEE Robot. Autom. Lett.*, early access, 2022, doi: 10.1109/LRA.2022.3192887.

[16] G. Taylor, "Analysis of the swimming of long and narrow animals," *Proc. Roy. Soc. London A, Math. Phys. Sci.*, vol. 214, no. 1117, pp. 158–183, 1952. [Online]. Available: http://www.jstor.org/stable/99081, doi: 10.1098/rspa.1952.0159.

[17] M. I. Lamas and C. G. Rodriguez, "Hydrodynamics of biomimetic marine propulsion and trends in computational simulations," *J. Mar. Sci. Eng.*, vol. 8, no. 7, p. 479, Jun. 2020, doi: 10.3390/jmse8070479.

[18] B. Sumer and J. Fredsøe, *Hydrodynamics Around Cylindrical Structures*, vol. 12. Singapore: World Scientific, Jan. 2006.

[19] A. Arbel, "Controllability measures and actuator placement in oscillatory systems," *Int. J. Control*, vol. 33, no. 3, pp. 565–574, 1981, doi: 10.1080/00207178108922941.

[20] M. Van De Wal and B. D. Jager, "A review of methods for input/output selection," *Automatica*, vol. 37, no. 4, pp. 487–510, 2001, doi: 10.1016/S0005-1098(00)00181-3.

Kai Junge, Computational Robot Design and Fabrication Lab, Swiss Federal Institute of Technology Lausanne, Lausanne 1015, Switzerland. E-mail: kai.junge@epfl.ch.

Nana Obayashi, Computational Robot Design and Fabrication Lab, Swiss Federal Institute of Technology Lausanne, Lausanne 1015, Switzerland. E-mail: nana.obayashi@epfl.ch.

Francesco Stella, Computational Robot Design and Fabrication Lab, Swiss Federal Institute of Technology Lausanne, Lausanne, Switzerland, and Department of Cognitive Robotics, Delft University of Technology, Delft 2628 CD, The Netherlands. E-mail: francesco.stella@epfl.ch.

Cosimo Della Santina, Department of Cognitive Robotics, Delft University of Technology, Delft 2628 CD, The Netherlands. E-mail: cosimodellasantina@gmail.com.

Josie Hughes, Computational Robot Design and Fabrication Lab, Swiss Federal Institute of Technology Lausanne, Lausanne 1015, Switzerland. E-mail: josie.hughes@epfl.ch.